This article has been accepted for publication in IEEE Antennas and Wireless Propagation Letters. This is the author's version which has not been fully edited and content may change prior to final publication. Citation information: DOI 10.1109/LAWP.2022.3210883



# Textile Bandwidth-Enhanced Half-Mode Substrate-Integrated Cavity Antenna With V-Slot for WLAN Communications

Feng-Xue Liu, Jie Cui, Jun Wang, *Member, IEEE*, and Lei Zhao, *Senior Member, IEEE*

***Abstract*—A textile bandwidth-enhanced half-mode substrate-integrated cavity (HMSIC) antenna is designed for the wireless local area network (WLAN) communications. Through simulations over the vector surface current on the top layer of a basic HMSIC antenna, a simple strategy of adding a slot on the top layer to shift the resonance frequency of the rotated $\mathbf{TM^{HM}_{2,2,0}}$ mode towards the counterpart of the fundamental $\mathbf{TM^{HM}_{1,1,0}}$ mode is presented. Based on that, the parameters of the slot are optimized to merge the two corresponding bands into one with an enhanced bandwidth. A prototype with a $0.35\times0.7\ \lambda_\varepsilon^2$ cavity is fabricated and measured to verify the design. The measured -10 dB impedance band is 5.04-5.90 GHz with a 15.7% factional bandwidth covering the 5 GHz WLAN band, and the radiation efficiency is above 94% in free space and 80% on the human body. Besides, the proposed antenna shows a high robustness against the human body and cylindrical bending conditions, and the simulated specific absorption rate (SAR) proves its safety on the human body.**

***Index Terms*—Textile antenna, substrate-integrated antenna, bandwidth enhancement, computerized embroidery.**

## I. Introduction

In recent years, the wearable antenna has been studied and applied in various areas including medical monitoring, sport training, defense and security [1–4]. The textile antenna is suitable for wearable applications because of its high flexibility, low weight and easy integration into clothes [5]. The half-mode substrate-integrated waveguide/cavity (HMSIW/HMSIC) antenna is a candidate geometry for the textile antenna because of its planar structure and small 2-D footprint [6, 7]. However, the fundamental-mode band of the HMSIW/HMSIC antenna is relatively narrow due to its high frequency selectivity due to the resonant cavity.

For the HMSIW/HMSIC antenna, adding shorting vias is an effective bandwidth enhancing method by reshape the internal E-field distribution of the lower resonance. Reference [8, 9] respectively introduced a rigid via-loaded HMSIW antenna and two textile via-loaded HMSIC antennas. For these antennas, the lower resonance frequency was increased by the added shorting vias while the higher resonance frequency remains unchanged until two bands were merged to enhance the bandwidth. Reference [10, 11] introduced another method to increase the bandwidth for the wearable planar inverted-F antenna (PIFA) by adding both slot and shorting vias. The slot reduced the higher-order resonance frequency while the shorting vias oppositely increased the lower-order resonance frequency until a widened band was obtained. In both methods, the resonance frequency of the lower-order mode, namely the fundamental mode, was increased by the added shorting vias. Therefore, in order to keep the lower resonance frequency unchanged, both methods demand larger cavities/patches which are disadvantageous for wearable applications. Besides, reference [12] introduced a flexible HMSIW cavity-backed antenna on cork substrate where a slot were added to introduce an extra resonance to enhance the bandwidth without significantly affecting the resonance frequency of the fundamental mode. This bandwidth enhancing method does not need larger cavities/patches, and thus provides inspirations for this letter.

This letter presents a textile bandwidth-enhanced HMSIC antenna with V-slot for WLAN communications. The vector surface current distributions on the top layer for a basic HMSIC antenna operating in the $\mathrm{TM}^{\mathrm{HM}}_{1,1,0}$ and rotated $\mathrm{TM}^{\mathrm{HM}}_{2,2,0}$ modes are simulated to identify the strategy of adding a slot to shift the higher-order resonance towards the lower-order resonance. Based on that, the geometrical parameters of the antenna and the slot are optimized to cover the 5 GHz WLAN band (5.15-5.825 GHz). The influences of the human body on the antenna performance and the SAR in the human body are investigated through simulations. A prototype is fabricated and measured to verify the design, and the effect of cylindrical bending conditions is studied through measurements.

## II. Geometry Design

### A. Basic HMSIC Antenna

Figure 1 (a) shows the geometry of a basic HMSIC antenna (Antenna I). Its cavity is defined by the conductive top layer, ground plane, sidewall and the radiation aperture. Losses of the top layer, ground plane, substrate and sidewall are considered in modelling to study the realistic bandwidth. Both the top layer and the ground plane are formed by the conductive fabric with a measured sheet resistance of 0.04 Ω/□. The substrate is selected as the PF-4 foam from Cumming Microwave with its thickness $h$ = 3.2 mm, relative permittivity $\varepsilon_r$ = 1.06 and loss tangent $\tan\delta$ = 0.0001. The vertical sidewall is built by linearly embroidering conductive threads (Shieldit 117/17 2PLY) for 3 passes with a stitch spacing of 2 mm. The equivalent sheet resistance of the sidewall is determined to be 0.6 Ω/□ based on the preliminary measurements. A copper probe with a 0.6 mm radius and a coaxial lumped port with

F.-X. Liu is with School of Physics and Electronic Engineering, Jiangsu Normal University, Xuzhou, Jiangsu 221116, China, and also with Jiangsu Xiyi Advanced Materials Research Institute of Industrial Technology, Xuzhou, Jiangsu 221400, China, and also with Jiangsu Normal University Kewen College, Xuzhou, Jiangsu 221132, China. email: liufengxue@jsnu.edu.cn

J. Cui, J. Wang and L. Zhao are with School of Information and Control Engineering, China University of Mining and Technology, Xuzhou, Jiangsu 221116, China. J. Cui is also with Jiangsu Vocational Institute of Architectural Technology, Xuzhou, Jiangsu 221116, China.

This work is supported by Natural Science Foundation of Jiangsu Province under Grant BK20221226, and also by Jiangsu College and University Natural Science Research Project under Grant 18KJB510014 and Grant 21KJB510030, and also by Xuzhou Science and Technology Project under Grant KC19002.

© 2022 IEEE. Personal use is permitted, but republication/redistribution requires IEEE permission. See https://www.ieee.org/publications/rights/index.html for more information.
Authorized licensed use limited to: CHINA UNIVERSITY OF MINING AND TECHNOLOGY. Downloaded on September 30,2022 at 02:16:25 UTC from IEEE Xplore. Restrictions apply.

This article has been accepted for publication in IEEE Antennas and Wireless Propagation Letters. This is the author's version which has not been fully edited and content may change prior to final publication. Citation information: DOI 10.1109/LAWP.2022.3210883



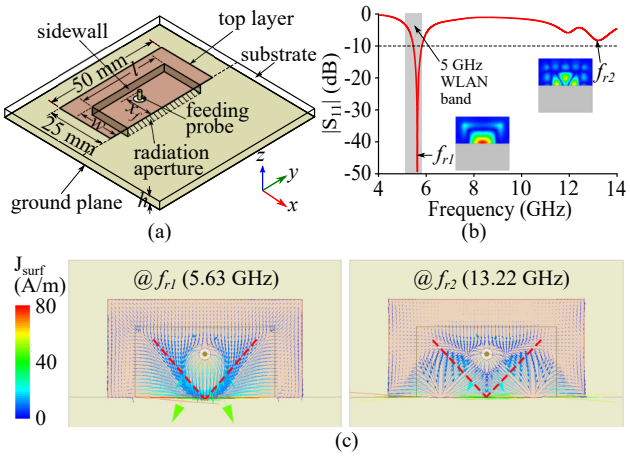


Fig. 1. Antenna I: (a) geometry; (b) simulated $|S_{11}|$ curve; (c) simulated vector surface current distributions on the top layer.

a 1.5 mm radius are modeled to imitate the feeding SMA connector. The ground plane is determined by be $70 \times 70$ mm$^2$ to provide isolation of the antenna and the human body. Based on simulations, $w$ = 18 mm, $l$ = 36 mm, and $x_f$ = 12 mm.

The simulated $|S_{11}|$ curve of Antenna I is shown in Fig. 1 (b). The first resonance is observed at $f_{r1}$ = 5.63 GHz, and the -10 dB band is 5.46-5.83 GHz which fails to cover the 5 GHz WLAN band. The second resonance is found at $f_{r2}$ = 13.22 GHz. The simulated internal E-field distributions at $f_{r1}$ and $f_{r2}$ as shown in the insets of Fig. 1 (b) indicate that Antenna I is operating in the half $TM_{1,1,0}$ (denoted as $TM^{HM}_{1,1,0}$) mode at $f_{r1}$ and half 45°-rotated $TM_{2,2,0}$ (denoted as rotated $TM^{HM}_{2,2,0}$) mode at $f_{r2}$ [9].

### B. Effect of Adding V-Slot

The simulated vector surface current on the top layer at $f_{r1}$ and $f_{r2}$ are shown in Fig. 1 (c). At $f_{r1}$, the vector current is nearly parallel to the V-shape path marked by the red dashed lines. At $f_{r2}$, however, the vector current is basically orthogonal to the path. It can be assumed that adding a slot along the V-shape path does not influence the current distribution of the first resonance while lengthens the current path of the second resonance and reduces $f_{r2}$. To validate the assumption, a HMSIC antenna with V-slot (Antenna II) is modelled as shown in Fig. 2. Parameters $w$, $l$ and $x_f$ and the size of the ground plane remain the same values of Antenna I for comparison, while $\alpha$ and $d$ are respectively determined to be 90° and 0.8 mm based on the rough measurement on Fig. 1 (c). Parametric studies (not shown due to limited space) indicate that both increasing $\alpha$ and decreasing $d$ can slightly increase the -10 dB bandwidth. The slot width $w_s$ is optimized to be 3 mm for the impedance matching at the second resonance.

The simulated $|S_{11}|$ curves of Antenna II with different values of $l_s$ are shown in Fig. 3. Compared to Antenna I, $f_{r1}$ of Antenna II slightly increases while $f_{r2}$ dramatically decreases. And the larger $l_s$, the closer $f_{r2}$ is to $f_{r1}$. When $l_s$ continues to increase, $f_{r2}$ can be even lower than $f_{r1}$. Therefore, it is feasible to adjust $l_s$ to shift $f_{r2}$ to slightly lower than $f_{r1}$ to merge the two bands into a one with an enhanced bandwidth in a relatively smaller cavity.

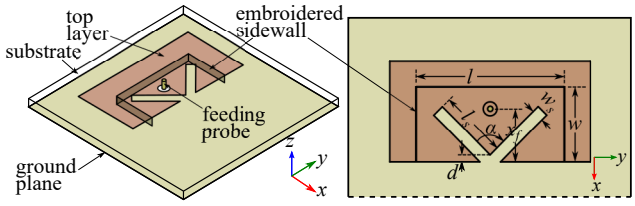


Fig. 2. Geometry of Antenna II.

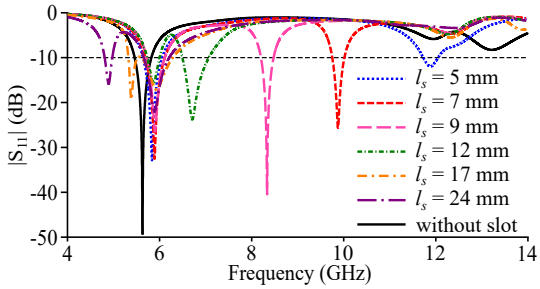


Fig. 3. Simulated $|S_{11}|$ curves of Antenna II with different values of $l_s$.

### C. Simulation Results of Antenna II

Through simulations, the parameters of Antenna II are re-optimized and determined as: $w$ = 18.5 mm, $l$ = 37 mm, $x_f$ = 12.5 mm, $\alpha$ = 90°, $d$ = 0.8 mm, $l_s$ = 17.5 mm and $w_s$ = 3 mm. The simulated $|S_{11}|$ curve of Antenna II with optimized parameter values in free space is shown in Fig. 4 (a). It can be observed that $f_{r2}$ and $f_{r1}$ are 5.21 and 5.62 GHz, respectively. And a -10 dB impedance band of 5.13-5.86 GHz (13.3% fractional bandwidth) is obtained to provide the coverage over the 5 GHz WLAN band.

The co-polarized gain patterns of Antenna II in free space at 5.15 GHz, $f_{r2}$ (5.21 GHz), 5.5 GHz, $f_{r1}$ (5.62 GHz) and 5.825 GHz are simulated and shown in Fig. 5 (a). At each of frequencies, the patterns shows a wide main beam in the positive hemisphere with a front-to-back ratio (FTBR) above 14.6 dB, and are therefore suitable for wearable applications. The simulated maximum gains at 5.15, 5.21, 5.5, 5.62 and 5.825 GHz are 3.1, 3.9, 5.3, 6.4 and 7.2 dBi, respectively. The curves of the maximum gain and the radiation efficiency of Antenna II with respect to the frequency are shown in Fig. 6. Cylindrical bending conditions as shown in the insets of Fig. 4 (b) are also modelled and simulated. In the whole 5 GHz WLAN band, the maximum gain is above 3.1 / 4.8 dBi in flat / bending condition, and the radiation efficiency is above 94% / 89% in flat / bending condition.

The effects of the human body are also studied. A $300 \times 300 \times 60$ mm$^3$ three-layer (skin-fat-muscle) human body model as shown in the inset of Fig. 4 (a) is employed, and each layers have the same characteristics and thicknesses as those in [9]. Antenna II is located above the center of the top surface of the human body model with a 5 mm distance. The simulated $|S_{11}|$ curve of Antenna II on the human body model is presented in Fig. 4 (a). The simulated resonance frequencies of Antenna

© 2022 IEEE. Personal use is permitted, but republication/redistribution requires IEEE permission. See https://www.ieee.org/publications/rights/index.html for more information.
Authorized licensed use limited to: CHINA UNIVERSITY OF MINING AND TECHNOLOGY. Downloaded on September 30,2022 at 02:16:25 UTC from IEEE Xplore. Restrictions apply.

This article has been accepted for publication in IEEE Antennas and Wireless Propagation Letters. This is the author's version which has not been fully edited and content may change prior to final publication. Citation information: DOI 10.1109/LAWP.2022.3210883



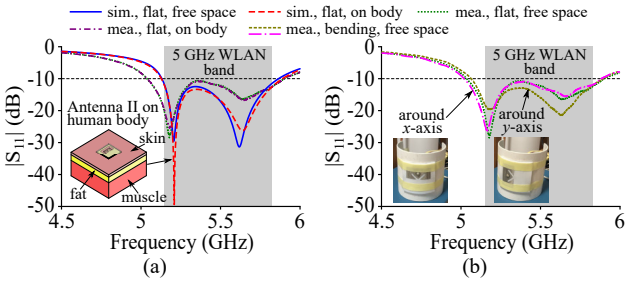


Fig. 4. Simulated and measured $|S_{11}|$ curves of Antenna II: (a) simulated and measured curves in flat condition; (b) measured curves in cylindrical bending conditions.

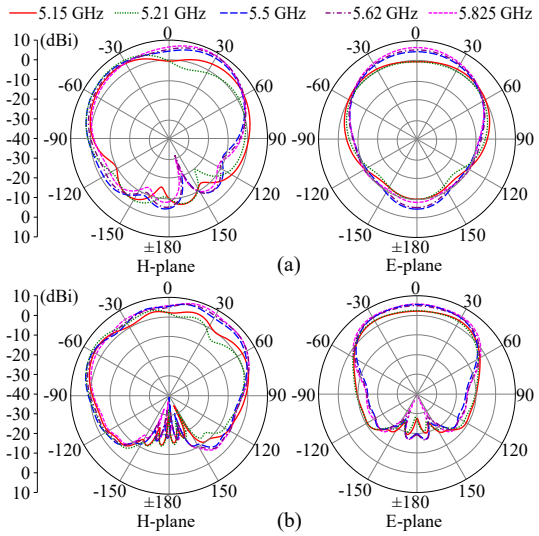


Fig. 5. Simulated co-polarized gain patterns of Antenna II: (a) in free space; (b) on human body model.

II on the human body model are 5.21 and 5.64 GHz, and the -10 dB impedance band is 5.13-5.89 GHz (13.8% fractional bandwidth). The high agreement between the two $|S_{11}|$ curves with/without the human body model illustrates the robustness of Antenna II against the human body.

The simulated co-polarized gain patterns, curves of the maximum gain and radiation efficiency with respect to the frequency for Antenna II on the human body model are shown in Fig. 5 (b) and Fig. 6, respectively. The simulated patterns with the human body model are still suitable for wearable applications a with wide positive main beam in the positive hemisphere, and show lower backward radiations because of the human body model as an extra ground plane. In the investigated 5 GHz WLAN band, the simulated maximum and radiation efficiency are above 3.1 dBi and 80%, respectively. The decrease of the efficiency can be explained by the radiation absorption of the human body as a lossy medium. The 1 g average SAR on the human body model with a standard 0.5 W input power [16, 17] is simulated at 5.15, 5.21, 5.5, 5.62 and 5.825 GHz (distributions not shown for brevity). The maximum values of the simulated SAR are 0.57, 0.60, 0.53, 0.50 and 0.39 W/kg at the five investigated frequencies, respectively, which are well below the limits of IEEE C95.1-2005 (1.6 W/kg) and EN 50361-2001 (2.0 W/kg),

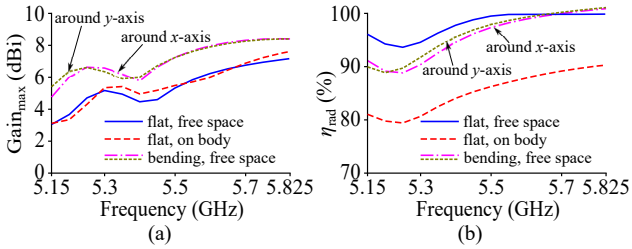


Fig. 6. Simulated curves of (a) the maximum gain and (b) the radiation efficiency of Antenna II in flat condition.

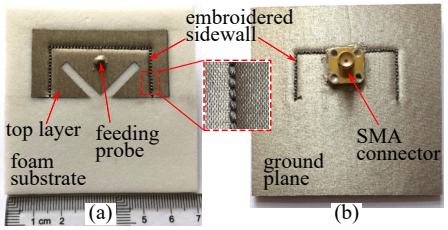


Fig. 7. Photos of fabricated textile prototype of Antenna II: (a) top view; (b) back view.

and therefore prove the safety of the proposed antenna.

## III. Prototype Fabrication and Measurements

A prototype of Antenna II as shown in Fig. 7 is fabricated with computerized embroidery machine Brother nv950. Conductive epoxy CW2460 from CircuitWorks is used install the feeding SMA connector.

The measured $|S_{11}|$ curves of the prototype in free space and on the human body are shown in Fig. 4 (a) with a reasonable agreement with simulation results. For two basically overlapping curves, $f_{r2}$ = 5.18 GHz, $f_{r1}$ = 5.64 GHz, and the -10 dB band is 5.04-5.90 GHz (15.7% factional bandwidth). Both curves show sufficient coverage over the 5 GHz WLAN band. The measured resonance frequencies are quite accurate compared to simulations. The measured -10 dB bandwidths are larger than expectations. It could be explained by the unconsidered losses in the prototype such as that of the conductive epoxy. The measured impedance matching is not as good as simulations at $f_{r2}$ due to the slight inaccuracy of the feeding position.

As shown in Fig. 8, the measured co-polarized gain patterns of the prototype in flat condition at all investigated frequencies are of suitable shapes for wearable applications, and show a reasonable agreement with simulations. The measured maximum co-polarized gains at 5.15, 5.21, 5.5, 5.62 and 5.25 GHz are 2.9, 4.8, 5.5, 7.0 and 7.1 dBi, respectively, and the corresponding FTBRs are above 13.6 dB. In practical applications, the backward radiation can be further reduced by using a larger ground plane which can be conductive fabric or conductive threads weaving in the clothes.

A PVC frame as shown in the in sets of Fig. 4 (b) is fabricated to provide a cylindrical surface for the bending condition. The measured $|S_{11}|$ curves with bending conditions in both considered directions are shown in Fig. 4 (b) with full coverage over the 5 GHz WLAN band, and thus indicate the robustness of the propose antenna against bending conditions.

© 2022 IEEE. Personal use is permitted, but republication/redistribution requires IEEE permission. See https://www.ieee.org/publications/rights/index.html for more information.
Authorized licensed use limited to: CHINA UNIVERSITY OF MINING AND TECHNOLOGY. Downloaded on September 30,2022 at 02:16:25 UTC from IEEE Xplore. Restrictions apply.

This article has been accepted for publication in IEEE Antennas and Wireless Propagation Letters. This is the author's version which has not been fully edited and content may change prior to final publication. Citation information: DOI 10.1109/LAWP.2022.3210883



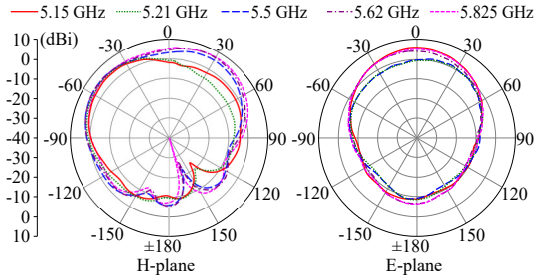


Fig. 8. Measured co-polarized gain patterns of Antenna II.

TABLE I
COMPARISON WITH OTHER SIMILAR WEARABLE BANDWIDTH ENHANCED SIW/HMSIW ANTENNAS

| Ref. | Freq. (GHz) | BW (%) | $\text{Gain}_{\max}$ (dBi) | $\eta_{\text{rad}}$ % | Cavity size ($\lambda_\varepsilon^2$) |
|---|---|---|---|---|---|
| [9] | 5.5 | 14.7 | 8.8 | $\geqslant 95$ | 1.073 |
| [11] | 5.5 | 18 | 5.9 | 74.1 | 0.662 |
| [12] | 5.5 | 23.7 | 4.3 | 85 | 0.364 |
| [13] | 2.45 | 16.2 | 4.7 | 67-82 | 0.096 |
| [14] | 2.45 | 6 | not given | not given | 0.220 |
| This work | 5.5 | 15.7 | 7.1 | $\geqslant 94$ | 0.245 |

## IV. CONCLUSIONS

A textile bandwidth-enhanced HMSIC antenna with V-slot for WLAN communications has been introduced. The strategy of adding the slot based on the surface currents provides a simple and effective method to enhance the bandwidth for the textile HMSIC antenna. The measurements over the prototype show a stable coverage over the 5 GHz WLAN band with/without the human body and bending conditions. The comparison between the proposed antenna and other similar flexible bandwidth-enhanced SIW/HMSIW antennas is shown in Table I. The bandwidth of the proposed antenna is lower than [11], [12] and [13] because of its low-loss PF-4 foam substrate [15]. However, the low overall loss of the proposed antenna also leads to the leading radiation efficiency and maximum gain. Besides, apart from [13] where two eighth-mode cavities were employed and resulted in the circular/elliptical polarization, the cavity of the proposed antenna is basically the smallest. Compared to our previous work [9], this work dramatically reduces the cavity size and slightly increases the bandwidth for the textile HMSIC antenna.

## REFERENCES

[1] A. Galehdar and D. V. Thiel, "Flexible, light-weight antenna at 2.4GHz for athlete clothing," in *Proc. APSURSI*, Honolulu, HI, USA, Dec, 2007, pp. 4160-4163.

[2] C. Hertleer, H. Rogier, L. Vallozzi and L. V. Langenhove, "A textile antenna for off-body communication integrated into protective clothing for firefighters," *IEEE Trans. Antennas Propag.*, vol. 57, no. 4, pp. 919–925, Apr. 2009.

[3] H. Lee, J. Tak and J. Choi, "Wearable Antenna Integrated into Military Berets for Indoor/Outdoor Positioning System," *IEEE Antennas Wireless Propag. Lett.*, vol. 16, pp. 1919-1922, Mar. 2017.

[4] X. Lin, Y. Chen, Z. Gong, B.-C. Seet, L. Huang and Y. Lu, "Ultra-wideband textile antenna for wearable microwave medical imaging applications," *IEEE Trans. Antennas Propag.*, vol. 68, no.6, pp. 4238–4249, Jun. 2020.

[5] K. N. Paracha, S. K. Abdul Rahim, P. J. Soh and M. Khalily, "Wearable antennas: a review of materials, structures, and innovative features for autonomous communication and sensing," *IEEE Access*, vol. 7, pp. 56694-56712, Apr. 2019.

[6] T. Kaufmann and C. Fumeaux, "Wearable textile half-mode substrate-integrated cavity antenna using embroidered vias," *IEEE Antennas Wireless Propag. Lett.*, vol. 12, pp. 805–808, Jun. 2013.

[7] F.-X. Liu, T. Kaufmann, Z. Xu and C. Fumeaux, "Wearable applications of quarter-wave patch and half-mode cavity antennas," *IEEE Antennas Wireless Propag. Lett.*, vol. 14, pp. 1478–1481, Dec. 2014.

[8] Y. Shi and J. Liu, "Investigation of a via-loaded microstrip magnetic dipole antenna with enhanced bandwidth and gain," *IEEE Trans. Antennas Propag.*, vol. 67, no. 7, pp. 4836–4841, Jul. 2019.

[9] J. Cui, F.-X. Liu, H. Yin and L. Zhao, "Textile via-loaded bandwidth-enhanced half-mode substrate-integrated cavity antenna for WLAN communications," *IEEE Trans. Antennas Propag.*, doi: 10.1109/TAP.2022.3161332.

[10] N.-W. Liu, L. Zhu and W.-W. Choi, "A low-profile wide-bandwidth planar inverted-F antenna under dual resonances: principle and design approach," *IEEE Trans. Antennas Propag.*, vol. 65, no. 10, pp. 5019–5025, Oct. 2017.

[11] G.-P. Gao, C. Yang, B. Hu, R.-F. Zhang and S.-F. Wang, "A wide-bandwidth wearable all-textile PIFA with dual resonance modes for 5 GHz WLAN applications," *IEEE Trans. Antennas Propag.*, vol. 67, no. 6, pp. 4206–4211, Jun. 2019.

[12] O. Caytan, S. Lemey, S. Agneessens, D. V. Ginste, P. Demeester, C. Loss, R. Salvado and H.Rogier, "Half-mode substrate-integrated-waveguide cavity-backed slot antenna on cork substrate," *IEEE Antennas Wireless Propag. Lett.*, vol. 15, pp. 162–165, Feb. 2016.

[13] S. Agneessens, "Coupled eighth-mode substrate integrated waveguide antenna: small and wideband with high-body antenna isolation," *IEEE Access*, vol. 6, pp. 1595-1602, Dec. 2017.

[14] S. P. Pinapati, D. C. Ranasinghe and C. Fumeaux, "Bandwidth enhanced dual-band half-mode substrate-integrated cavity antenna," in *Proc. AMS*, Brisbane, Australia, Feb. 2018, pp. 51-52.

[15] A. Yaghjian and S. Best, "Impedance, bandwidth, and Q of antennas," *IEEE Trans. Antennas Propag.*, vol. 53, no. 4, pp. 1298–1324, Apr. 2005.

[16] ICNIRP, "Guidelines for limiting exposure to time-varying electric, magnetic, and electromagnetic fields (up to 300 GHz)," *Health physics*, vol. 118, no. 5, pp. 483-524, 2020.

[17] IEEE Std, *IEEE Standard for Safety Levels with Respect to Human Exposure to Electric, Magnetic, and Electromagnetic Fields, 0 Hz to 300 GHz*. IEEE: New York, NY, USA, 2019.

© 2022 IEEE. Personal use is permitted, but republication/redistribution requires IEEE permission. See https://www.ieee.org/publications/rights/index.html for more information.
Authorized licensed use limited to: CHINA UNIVERSITY OF MINING AND TECHNOLOGY. Downloaded on September 30,2022 at 02:16:25 UTC from IEEE Xplore. Restrictions apply.